PDSim: A general quasi-steady modeling approach for positive displacement compressors and expanders

Ian H. Bell[a,b,*], Davide Ziviani[a], Vincent Lemort[b], Craig R. Bradshaw[c], Margaret Mathison[d], W. Travis Horton[a], James E. Braun[a], Eckhard A. Groll[a]

[a] *Center for High Performance Buildings, Purdue University, Ray W. Herrick Laboratories, 177 S. Russell Street, West Lafayette, IN 47907-2099, US*

[b] *University of Liège, Energy Systems Research Unit, Liège, Belgium*

[c] *Building, Environmental and Thermal Systems Research Group, Department of Mechanical and Aerospace Engineering, Oklahoma State University, Stillwater, OK 74074*

[d] *Department of Mechanical Engineering, Iowa State University, Ames, IA 50011*

Abstract

A novel generalized framework is presented that can be used to simulate the quasi-steady-state performance of a wide range of positive displacement compressors and expanders (scroll, piston, screw, rotary, spool, etc.). The complete simulation algorithm is described, and an emphasis is placed on the numerical methods required to obtain robust behavior of the simulation. This formulation has been implemented into an open-source software package entitled PDSim written in the Python language. PDSim is the first open-source generalized compressor and expander simulation package and the complete source code is included in the supplemental material. A piston expander is used as an example of the utilization of this framework. The framework has been applied to several positive displacement machines in the companion paper in order to demonstrate the flexibility of the approach (Ziviani et al. (2019)).

Keywords:
Positive displacement machines, Compressors, Expanders, Modeling, PDSim

1. Introduction

The detailed simulation of positive displacement compressors and expanders is of great interest, both academically and industrially. These simulation programs are typically developed in order to conduct computer-based prototyping; that is, with a properly tuned and validated model, it is possible to accurately predict the performance of the machine at conditions that the machine has not been tested at previously. Additionally, through the use of a model that is mechanistic, the actual performance can be predicted at operating conditions quite different than those at which the machine had been previously tested.

One of the shortcomings of many of the existing simulation codes for positive displacement machines is that they are highly specific, generally having been developed for a particular type of machine (scroll, reciprocating, etc.) and are typically structured in a way that makes the simulations very difficult to modify. Also, many of the simulation codes that have been developed are highly proprietary, which means that there is a large amount of simulation code development that is duplicative amongst industrial entities and academic researchers.

In this paper, a generalized framework for the simulation of positive displacement compressors and expanders is described. The full source code for the framework is also provided in the supplemental material. In the accompanying paper, examples (and the necessary source code) are provided for a wide range of different machines, demonstrating the flexibility of this framework, and investigating some of the challenges involved in simulating these types of devices.

There are a number of steady-state simulation codes described in the literature that have been tailor-made for a single type of positive displacement machine. A selection of the simulation codes developed over the last few decades are summarized in Table

There are also a number of simulation codes in use in industry, though the details are, in general, not in the public domain. The type of model described in this paper is sometimes also referred to as a chamber or 0-D model in the literature on compressors and expanders. The scope of the framework described here is the compression/expansion of pure compressible gases or mixtures thereof (i.e., no oil)

The original motivation for the development of PDSim was that positive displacement compressors and expanders

*Corresponding Author
Email addresses: ian.h.bell@gmail.com (Ian H. Bell), dziviani@purdue.edu (Davide Ziviani), vincent.lemort@ulg.ac.be (Vincent Lemort), craig.bradshaw@okstate.edu (Craig R. Bradshaw), mm1@iastate.edu (Margaret Mathison), wthorton@purdue.edu (W. Travis Horton), jbraun@purdue.edu (James E. Braun), groll@purdue.edu (Eckhard A. Groll)

NOMENCLATURE

Roman

A_c	Surface area of chamber (m^2)
A_tube	Cross-sectional area of tube (m^2)
A_valve	Frontal area of valve (m^2)
A_shell	Shell area (m^2)
c_p	Spec. heat at const. pressure (kJ kg^{-1} K^{-1})
c_v	Spec. heat at const. volume (kJ kg^{-1} K^{-1})
C_D	Valve drag coefficient (-)
D	Diameter (m)
D_h	Hydraulic diameter (m)
D_port	Diameter valve port (m)
D_valve	Diameter valve plate (m)
f	Friction factor (-)
G	Mass flux (kg m^{-2} s^{-1})
h	Specific enthalpy (kJ kg^{-1})
$h_\mathrm{d,chambers}$	Specific enthalpy of discharge (kJ kg^{-1})
h	Step size (s,radian)
h_c	Convective heat transfer coefficient (W m^{-2} K$^-$1)
$\mathbf{J}$	Jacobian
k	Thermal conduct. (kW m^{-1} K^{-1})
k_valve	Valve spring coefficient (N m^{-1})
L	Length (m)
m	Mass (kg)
m_valve	Valve mass (kg)
$\dot{m}_i$	Mass flow rate flow path (kg s^{-1})
$\dot{m}_\mathrm{tube}$	Mass flow rate in tube (kg s^{-1})
Δp	Change in pressure (Pa)
p	Pressure (kPa)
p_in	Inlet pressure (kPa)
p_out	Outlet pressure (kPa)
Pr	Prandtl Number (-)
$\dot{Q}$	Heat transfer rate (kW)
$\dot{Q}_\mathrm{amb}$	Heat transfer rate with ambient (kW)
$\dot{\vec{x}}_0, \dot{\vec{x}}_1, ...$	Time derivative of $\vec{x}_0, \vec{x}_1$..
$\vec{r}$	Residual array
r_ave	Average radius (m)
Re	Reynolds number (-)
t	Time (s)
s_in	Inlet specific entropy (kJ kg^{-1} K^{-1})
T	Temperature (K)
T_out	Outlet temperature (K)
T_in	Inlet temperature (K)
T_wall	Wall temperature (K)
U	Total internal energy (kJ)
V	Volume (m^3)
V_disp	Displacement volume (m^3)
V_dead	Dead volume (m^3)
$\mathbf{V}$	Flow velocity (m s^{-1})
$\dot{W}$	Power (kW)
$\dot{W}_\mathrm{bearing}$	Bearing Power (kW)
$\dot{W}_\mathrm{elec}$	Electrical Power (kW)
$\dot{W}_\mathrm{mech}$	Mechanical Power (kW)
$\dot{W}_\mathrm{mech,loss}$	Mechanical loss power (kW)
$\dot{W}_\mathrm{pV}$	Boundary work rate (kW)
$\dot{W}_\mathrm{s}$	Isentropic power (kW)
$\vec{x}_0, \vec{x}_1, ...$	State variable array
y	Valve position (m)
$\dot{y}$	Time deriv. valve disp. (m s^{-1})
$\ddot{y}$	Second time deriv. valve disp. (m s^{-2})
y_tr	Transit. valve disp. (m)

Greek

$\varepsilon_\mathrm{step}$	Step convergence criterion
ε_d	Discharge convergence criterion
$\varepsilon_\mathrm{cycle}$	Cycle convergence criterion
η_motor	Motor efficiency (-)
$\eta_\mathrm{s,mech}$	Expander isentropic efficiency (-)
μ	Viscosity (Pa s)
ω	Rotational speed (rad s^{-1})
ω_n	Natural frequency (s^{-1})
ω_nom	Nominal rotational speed (rad s^{-1})
θ	Crank angle (rad)
ρ	Density (kg m^{-3})
ε	Surface roughness (m)
$\tau_\mathrm{mech,loss}$	Mechanical loss torque (N m)

Table 1: List of mechanistic models published in the literature for different compressor and expander types

Machine Type	Compressor	Expander
Reciprocating and Linear		
Reciprocating	Link and Deschamps (2011),Yang et al. (2013); Hu et al. (2014)	Wronski (2015)
S-RAM	Yang et al. (2015)	N/A
Swash plate[a]	Tian et al. (2004)	Galindo et al. (2016), Oudkerk (2016)
Linear	Kim et al. (2009); Bradshaw et al. (2011); Bradshaw (2012)	N/A
Orbiting		
Scroll	Chen et al. (2002a,b); Bell (2011)	Lemort (2008); Lemort et al. (2008); Bell et al. (2012)
Trochoidal	Beard (1985); Shung and Pennock (1994)	N/A
Wankel	Zhang and Wang (2011)	Fransesconi and Antonelli (2017)
Rotary		
Cross-vane	Yap et al. (2018)	
Rolling-piston	Ooi and Wong (1997); Mathison et al. (2008)	Zhao et al. (2014)
Sliding-vane	Bianchi and Cipollone (2015)	N/A
Spool	Bradshaw and Groll (2013), Mathison et al. (2013)	Krishna (2015)
Swing-vane	Yang et al. (2017); Pan et al. (2018)	N/A
Screw		
Single-screw	Wang et al. (2018)	Ziviani (2017)
Twin-screw	Zaytsev (2003); Stosic et al. (2011)	Papes et al. (2016), Nikolov and Brummer (2017), Bianchi et al. (2018)
Novel		
Bowtie	Kim (2005)	N/A
Diaphragm	Sathe (2008)	N/A
Z	Jovane (2007); Ziviani and Groll (2017)	N/A

a: Sometimes also referred to as wobble plate

have significant overlap in their construction. Therefore, there is utility in a tool that models the common features shared amongst all types, this includes:

- Control volumes, which form the heart of the device and the model. These control volumes (working chambers) have volume profiles governed by the geometry. The change in volume of the working chambers results in compression (with power input) or expansion (with power recovery). The control volumes exchange heat and mass with the elements with which they communicate, as shown in Figure
  To the authors' knowledge, there has never been a generalized simulation code developed for all types of positive displacement compressors and expanders that is fully open-source.

2. Component Models

2.1. Thermophysical and transport properties

Before describing the component models in detail, it is necessary to first discuss the models used for the thermophysical properties of the working fluid(s) in the machine. The accuracy of the outputs of the simulation code are intimately linked to the accuracy of the thermophysical property models. Thermophysical properties of the working fluid are used in nearly all the component models and often constitute more than 90% of the running time of the simulation code. The CoolProp property library (Bell et al., 2014) is used to obtain the necessary thermodynamic and transport properties. Furthermore, a secondary property library derived from CoolProp has been included to retrieve properties of lubricant oil or other flooding mediums and their mixtures. In some cases, particularly for mixtures of refrigerants or for fluids not covered in CoolProp, the REFPROP thermophysical property library (Lemmon et al., 2016) can be used as the thermophysical property engine, and is called through the CoolProp interface. In order to speed up the evaluation of properties of mixtures of predefined composition, tabular interpolation can be employed, as demonstrated in Ziviani et al. (2019).

2.2. Control volume

A control volume, shown generically in Figure

– Uniform temperature and pressure throughout the control volume
– Negligible change of kinetic energy of the control volume
– Negligible gravitational effects
– Thermal interaction possible through heat transfer
– Mass flow into or out of control volume possible through a number of flow paths

This generic control volume, shown in Figure

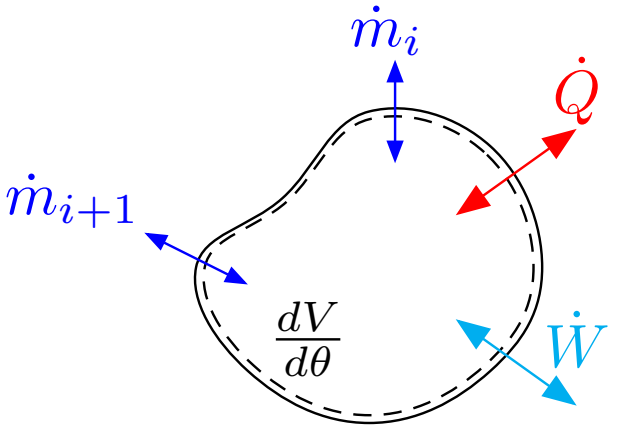

Figure 1: Schematic of generic control volume of a compressor or expander at crank angle of θ

Two independent, intrinsic, thermodynamic properties are needed to fix the thermodynamic state for pure fluids and fluid mixtures that are treated like pure fluids (see Lemmon(2003)). As will be presented in the following section, the derivatives of these two properties as a function of crank angle are needed. These derivatives will then be implemented into the solver that is used to calculate the properties throughout the course of a cycle. Thus, the formulation of the derivative expressions used in the solver depend on the selection of the two thermodynamic state variables.
Temperature and pressure are a physically consistent and easily-comprehensible set of state variables, but they are not well suited for positive displacement machine simulation. For instance, if the fluid passes into the two-phase region during the working process due to pressure drop or wet expansion, temperature and pressure are no longer independent and therefore can not be used to define the thermodynamic state.
The equations of state used in CoolProp and REFPROP are all of the Helmholtz energy explicit formulation and have as independent variables temperature and density. Therefore, temperature and density are the most straightforward state variables to use in the analysis that follows.
Mass and specific internal energy are also a viable pair of state variables (the most convenient from the standpoint of the conservation of energy and mass in a control volume), but difficulty arises from the fact that the equations of state are explicit in temperature and density rather than density and specific internal energy and it is therefore necessary to numerically solve for the temperature given the internal energy. The computational effort required to carry out this calculation is significant.
The conservation of mass for the control volume yields the following form for the time derivative of the mass in the control volume

$$\frac{\mathrm{d}m}{\mathrm{d}t} = \sum_i \dot{m}_i. \tag{1}$$

where $\dot{m}_i$ is the mass flow rate for the i-th flow path. For rotational machines working in the crank-angle domain, the derivative of the mass with respect to the crank angle can instead be given by,

$$\frac{\mathrm{d}m}{\mathrm{d}\theta} = \frac{1}{\omega}\sum_i \dot{m}_i \tag{2}$$

where $\dot{m}_i$ is the mass flow rate corresponding to the i-th flow path and ω is the rotational speed. The sign of $\dot{m}_i$ is positive if flow is into the control volume. Conservation of energy is given by,

$$\frac{\mathrm{d}U}{\mathrm{d}t} = \dot{Q} + \dot{W} + \sum_i \dot{m}_i h_i \tag{3}$$

where positive $\dot{Q}$ is heat flowing *into* the control volume, the boundary work term $\dot{W}$ is given by $\dot{W} = -p\cdot(\mathrm{d}V/\mathrm{d}t)$, and $\dot{m}_i h_i$ is the enthalpy flow term corresponding to the product of the upstream enthalpy and the mass flow rate for the i-th flow path. Expansion of the derivative of the total internal energy as in Bell (2011) allows for an analytic transformation from $\mathrm{d}U/\mathrm{d}t$ to $\mathrm{d}T/\mathrm{d}t$. This yields

$$\frac{\mathrm{d}T}{\mathrm{d}t} = \frac{-T\left(\frac{\partial p}{\partial T}\right)_\rho\left[\frac{\mathrm{d}V}{\mathrm{d}t} - \frac{1}{\rho}\frac{\mathrm{d}m}{\mathrm{d}t}\right] - h\frac{\mathrm{d}m}{\mathrm{d}t} + \dot{Q} + \sum_i \dot{m}_i h_i}{mc_v}, \tag{4}$$

and the crank-angle derivative of temperature can be obtained from

$$\frac{\mathrm{d}T}{\mathrm{d}\theta} = \frac{-T\left(\frac{\partial p}{\partial T}\right)_\rho\left[\frac{\mathrm{d}V}{\mathrm{d}\theta} - \frac{1}{\rho}\frac{\mathrm{d}m}{\mathrm{d}\theta}\right] - h\frac{\mathrm{d}m}{\mathrm{d}\theta} + \frac{\dot{Q}}{\omega} + \frac{1}{\omega}\sum_i \dot{m}_i h_i}{mc_v}. \tag{5}$$

The conversion from $\mathrm{d}U/\mathrm{d}t$ to $\mathrm{d}T/\mathrm{d}t$ is carried out because all the terms in Eq.
The geometric terms V and $\mathrm{d}V/\mathrm{d}\theta$ (or $\mathrm{d}V/\mathrm{d}t$) are given by the geometry of the machine. In the case of a piston machine, the geometry modeling is straightforward, while in the case of other more complex machines like screw and scroll compressors, calculation

of the necessary geometric terms is very involved. For that reason, no further analysis of the geometry is presented here, though characteristic plots of volume versus crank angle for a scroll compressor can be seen in Bell (2011).

2.3. Instantaneous Heat Transfer

The instantaneous heat transfer term $\dot{Q}$ is machine specific and depends on the geometry as well as the operating conditions. The sign of $\dot{Q}$ has been selected such that it is positive if the heat transfer is *into* the control volume. The instantaneous heat transfer is typically modeled as convective heat transfer, using Newton's Law of cooling

$$\dot{Q} = h_c A_c (T_{\text{wall}} - T) \tag{6}$$

where h_c is the convective heat transfer coefficient, A_c is the instantaneous surface area of the modeled chamber, and T_{wall} is the temperature of the wall surrounding the chamber.
The calculation of h_c is based on various heat transfer correlations which are specific to a type of machine type. Many of these correlations were developed for forced convection and have a general form of

$$h_c = a \frac{k}{D_h} \text{Re}^b \text{Pr}^c \tag{7}$$

where k is the thermal conductivity of the fluid, D_h is the hydraulic diameter of the chamber and Re and Pr are the Reynolds and Prandtl numbers, respectively. The parameters a, b, and c are generally experimentally obtained and depend on the fluid, geometry, and operating conditions. A selection of heat transfer correlations and their respective applications are given in Table

2.4. Fluid Flow Components

2.4.1. Tube

A tube is a component of the simulation that allows for pressure drop and heat transfer. It is modeled as being quasi-steady, and either the outlet or the inlet state is fixed. The following assumptions are employed:

- Steady state and steady flow
- Fixed wall temperature, fixed wall heat transfer flux, or user-defined heat transfer model
- Viscous effects present
- Single-phase flow enforced through the tube

The flow through the tubes is generally turbulent, and thus the friction factor can be given by the form from Churchill (1977),

$$f = 8 \left[(8/\text{Re})^{12} + (A+B)^{-1.5} \right]^{\frac{1}{12}} \tag{8}$$

$$A = \left(2.457 \ln \left[(7/\text{Re})^{0.9} + 0.27\,(\epsilon/D) \right]^{-1} \right)^{16} \tag{9}$$

$$B = (37530/\text{Re})^{16}\,. \tag{10}$$

The heat transfer coefficient can be given by the equation of Gnielinski (1975),

$$h_c = \frac{k}{D} \frac{(f/8)(\text{Re} - 1000)\text{Pr}}{1 + 12.7\sqrt{f/8}(\text{Pr}^{2/3} - 1)}. \tag{11}$$

The properties are evaluated at the known state. The Reynolds number is given by $\text{Re} = GD/\mu$, where G is the mass flux given by $G = \dot{m}_{\text{tube}}/A_{\text{tube}}$ and A_{tube} is the cross-sectional flow area of the tube given by $A_{\text{tube}} = \pi D^2/4$. If the inlet state of the tube is given and the wall temperature is known, the outlet temperature can be calculated from

$$T_{\text{out}} = T_{\text{wall}} - (T_{\text{wall}} - T_{\text{in}}) \exp\left(-\frac{\pi D L h_c}{\dot{m}_{\text{tube}} c_{\text{p}}} \right) \tag{12}$$

and the change in pressure by

$$\Delta p = -\frac{f G^2 L}{2\rho D}, \tag{13}$$

which yields the outlet pressure of $p_{\text{out}} = p_{\text{in}} + \Delta p$. If instead the outlet state is known, the inlet temperature can be calculated from Eq.

2.4.2. Flow Path

A flow path connects two flow nodes. These flow nodes could be control volumes, or they could be the inlet or an outlet for a tube section. In a flow path, the upstream state is fully specified and in general the downstream pressure is known. The model for the flow path must then calculate the mass flow rate through the flow path.
There are a wide range of flow models that can be employed for a flow path. The flow model selected depends on the geometry, flow type, and other parameters. It is also important to use different flow models if the flow can be treated as being compressible or not. Table

2.4.3. Valve

In some machine types, valves are required to ensure that the flow goes in the desired direction (e.g., piston compressors and expanders). In others (e.g., high pressure-ratio scroll compressors), valves are employed to reduce the re-expansion losses due to undercompression.
There are a number of different types of valves that exist in positive displacement machines, the most common type are dynamic reed valves because they are straightforward to fabricate. Kinematic valves (poppet valves) driven by the kinematics of the machine

Table 2: List of some heat transfer correlations used in literature and the accompanying technologies.

Correlation	Reference	Technology Type
$h_c = 0.053\frac{k}{D_h}\mathrm{Re}^{0.8}\mathrm{Pr}^{0.6}$	(Adair et al., 1972)	Reciprocating
$h_c = 0.75\frac{k}{D_h}\mathrm{Re}^{0.8}\mathrm{Pr}^{0.6}$	(Liu and Zhou, 1984)	Reciprocating, Rotary (Tan and Ooi, 2011)
$h_c = 0.023\frac{k}{D_h}\mathrm{Re}^{0.8}\mathrm{Pr}^{0.4}\left[1 + 1.77\frac{D_h}{r_{\mathrm{ave}}}\right]$	(Kakaç et al., 1987)	Scroll (Chen et al., 2002a)

Table 3: List of some flow models used in literature

Type	Reference	Compressible	Friction	Notes
Isentropic nozzle	(Bell et al., 2013)	Yes	No	Most common model, overpredicts flow rate, simple to implement
Incompressible pipe flow	(Ishii et al., 1996)	No	Yes	
Fanno flow	(Suefuji et al., 1992)	Yes	Yes	
Nozzle/Fanno combination	(Tojo et al., 1986)	Yes	Yes	
Superposition method	(Afjei et al., 1992)	No	Yes	
Hybrid leakage	(Bell et al., 2013)	Yes	Yes	Very computationally efficient, intended only for leakage

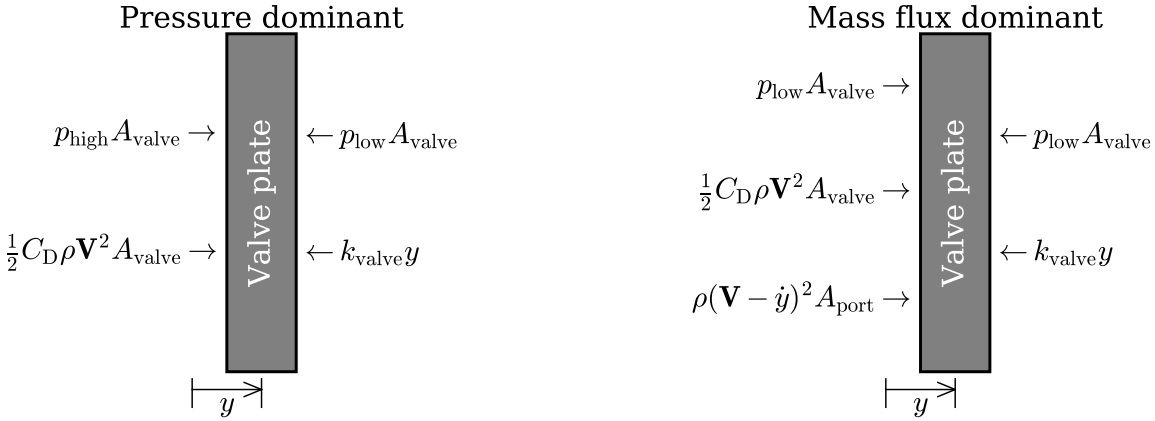

Figure 2: Free-body-diagrams for the valve plate of a dynamic reed valve in pressure-dominant and mass-flux dominant modes.

are also possible; kinematic valves are more straightforward to analyze as their opening and closing profiles are deterministic and are not governed by dynamics.

Although the reed valve dynamics and vibrational mode behavior can get quite complex (Soedel, 1984, 2007), reed valves are most often analyzed as one-degree-of-freedom, lumped element, vibrational systems (Kim, 2005; Bradshaw, 2012) as seen in Figure

Two modes of operation are considered, i.e., mass-flux dominant or pressure dominant, and the free-body-diagrams for the valve plate in each mode are shown in Figure

The second-order differential equation in y that governs the valve motion can be decoupled into two differential equations, one for y and another for $\dot{y}$, where $\dot{y}$ is the time-derivative of y (Suefuji and Nakayama, 1980; Kim, 2005). The derivatives of y and $\dot{y}$ are needed for the cycle integrator as described below. Therefore, it is only necessary to obtain $\ddot{y}$ in each domain because the derivative of y is simply $\dot{y}$.

In the mass flux dominant domain, the time derivative of $\dot{y}$ is given by

$$\ddot{y} = \frac{\frac{1}{2}C_{\mathrm{D}}\rho\mathbf{V}^2A_{\mathrm{valve}} + \rho(\mathbf{V}-\dot{x})^2A_{\mathrm{port}} - k_{\mathrm{valve}}y}{m_{\mathrm{valve}}} \tag{14}$$

and in the pressure dominant domain, the time derivative of $\dot{y}$ is given by

$$\ddot{y} = \frac{\frac{1}{2}C_{\mathrm{D}}\rho\mathbf{V}^2A_{\mathrm{valve}} + (p_{\mathrm{high}} - p_{\mathrm{low}})A_{\mathrm{valve}} - k_{\mathrm{valve}}y}{m_{\mathrm{valve}}} \tag{15}$$

The flow velocity $\mathbf{V}$ is calculated with the equation for isentropic flow of a compressible ideal gas through a nozzle with throat diameter equal to valve port diameter (velocity is calculated as though the valve plate

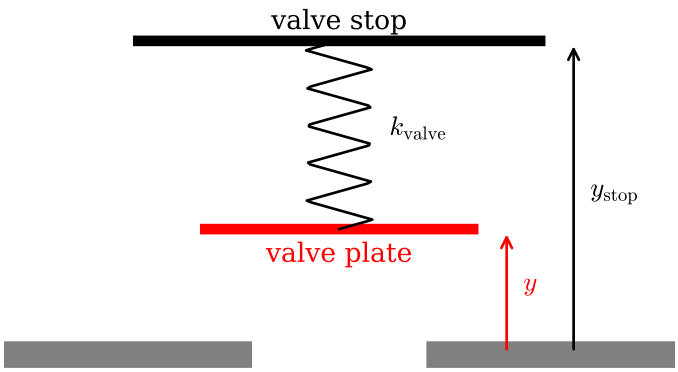

Figure 3: Reed valve diagram

was not present). The valve is usually constrained by two rigid bodies, the valve seat and the valve stop. If the integration leads to $y < 0$ or $y > y_{\text{stop}}$, the displacement of the valve is set to 0 or y_{stop}, respectively.

2.5. Mechanical System

The chambers of the positive displacement machine are embedded into a larger mechanical system that allows for bi-directional conversion between electrical (or rotational) power and boundary work in the chambers of the machine. The conversion between electrical energy and mechanical energy is carried out with a motor (when running in the reverse direction, motors are referred to as generators). In an ideal machine, this conversion is carried out reversibly, without any mechanical losses. In reality, the motor has losses associated with the conversion of work and the mechanism used to perform boundary work has irreversibilities associated with it as well. For example, the contact of two surfaces under applied load, or the shearing of a liquid (as in the oil in a bearing) results in irreversibility. This irreversibility manifests as a heat source and a decrease in efficiency. PDSim includes modules which describe a variety of potential mechanical losses including motor losses, bearing losses, and other frictional losses.

2.5.1. Mechanical Analysis and Friction Losses

The mechanical analysis of the compressor motion allows for the determination of the forces and moments acting on the mechanical components such as shaft, bearings, sliding vanes, etc., which are particular for each compressor type. The friction losses of dynamic components are coupled into the dynamic analysis of the mechanical components. Examples of such analyses applied to different machines can be found in the open literature:

- Scroll compressor (Liu et al., 2010; Bell, 2011)
- Rotary compressor: rolling piston (Okada and Kuyama, 1982; Yanagisawa and Shimizu, 1985); sliding vane (Bianchi and Cipollone, 2015); spool (Bradshaw et al., 2016); z-compressor (Jovane, 2007)
- Reciprocating compressor (Singh, 1984; Link and Deschamps, 2011)
- Screw compressor (Wu and Tran, 2016)

PDSim includes the possibility of implementing detailed mechanical analyses to estimate each frictional contribution

$$\dot{W}_{\text{friction}} = \sum_i \dot{W}_{\text{friction},i} \tag{16}$$

In the absence of a mechanistic model for mechanical losses, it is possible to correlate the mechanical losses to the gas compression power and obtain an empirical relationship for the mechanical efficiency (Liu et al., 2010). This correlation is constructed by first running the model with input state points for which experimental data are available, with no mechanical losses or heat transfer. The residual between the model predicted shaft power and the experimental shaft power is then assumed to be due to mechanical losses. A correlation of the form

$$\dot{W}_{\text{mech,loss}} = \omega \tau_{\text{mech,loss}} \tag{17}$$

is fit to the data for the compressor or expander and the loss coefficient $\tau_{\text{mech,loss}}$ is obtained.

2.5.2. Bearings

There are two primary families of bearings in positive displacement machines - journal bearings and slider bearings, as seen in Figure

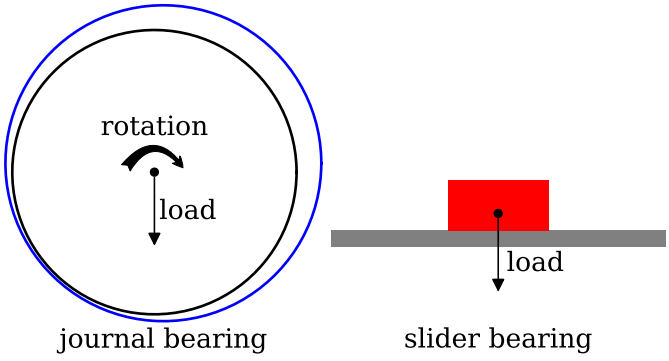

Figure 4: Schematics of journal (left) and slider (right) bearings (see Figures 8.3 and 10.1 in Hamrock et al. (2004), respectively).

Journal bearings consist of a rotating shaft (or journal) rotating in a bearing (or alternatively, a fixed shaft inside a rotating housing) with a layer of lubricant separating the two parts. These types of bearings are commonly found in the support structure for the drive shaft of hermetic compressors and expanders, with an oil supply provided by an oil pump. An oilless version of this type of bearing is referred to as a

gas or foil bearing and is used in very high speed applications (Hamrock et al., 2004; Schiffmann, 2014). For finite-length, oil-lubricated, journal bearings, it is possible to utilize the numerical solutions of Raimondi and Boyd (1958a; 1958b; 1958c), or to use the Sommerfeld analytic solutions (Hamrock et al., 2004). Slider bearings include any type of bearing where two surfaces are sliding against each other with an applied normal force. This could be the thrust bearing of a scroll compressor, or the point of contact of the Oldham coupling of a scroll compressor. Slider bearings are characterized by a friction coefficient, where the friction coefficient is calculated based on simple models (constant friction coefficient) or semi-empirical/theoretical models based on the loading of the bearing surface.

2.5.3. Motor

A motor is generally characterized by its slip speed, its electrical input power and its delivered mechanical torque. Motor manufacturers typically provide motor efficiency and slip speed curves or tabulated data as a function of the mechanical torque delivered. The slip speed is always less than the frequency of the applied electrical signal and it is given by

$$\omega = (1 - s)\,\omega_{\text{nom}} \tag{18}$$

where s is the slip ratio usually in the range from 0.001 and 0.2 and ω_{nom} is the angular speed corresponding to the nominal frequency of the electric signal.
Three different models are considered within PDSim:

- Motor with constant efficiency
- Motor efficiency as a function of torque and slip velocity
- Semi-deterministic model of the motor including heat and friction losses

The mechanical power output of the motor is given by $\dot{W}_{\text{mech}} = \omega\tau$ and the efficiency is given by

$$\eta_{\text{motor}} = \frac{\dot{W}_{\text{mech}}}{\dot{W}_{\text{elec}}} \tag{19}$$

The fraction of the electrical power that is not converted to mechanical power is lost as heat, as shown in Figure
When the motor is run in reverse as an electrical generator, similar analysis applies.

3. Numerical Analysis

At the heart of every model is the set of control volumes, the working chambers in the machine. The state of the control volumes at the beginning of the simulation is known from the initialization of the model, and a system of tightly-coupled differential

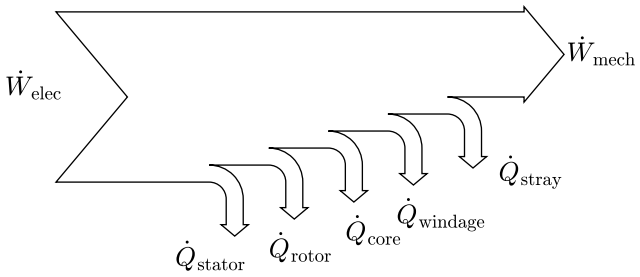

Figure 5: Sankey diagram of the power flow of a single-phase induction motor (Chapman, 2005).

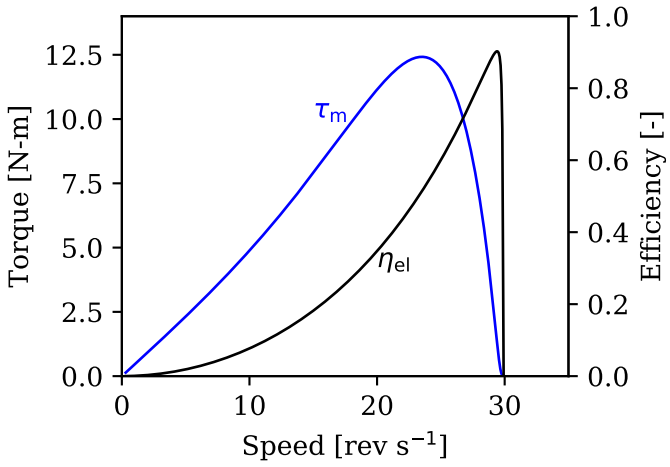

Figure 6: Torque-efficiency-speed characteristic of a single-phase induction motor.

equations describes the future behavior of the machine. In order to obtain the temperature, pressure, density, etc. of the gas in the control volumes over the course of the cycle, it is necessary to integrate the coupled, non-linear system of equations arising from the differential forms of conservation of mass and energy. The set of differential equations can be expressed in the functional form

$$\dot{\vec{x}} = \dot{x}(t, \vec{x}) \tag{20}$$

where t is the variable of integration, and $\vec{x}$ is the array of state variables and other variables that are involved in the integration. As an example, for a machine with two control volumes A and B that employ two dynamic valves 1 and 2, assuming the thermodynamic state variables that are used are T and ρ, the array $\vec{x}$ and the time-derivative of the array $\vec{x}$ are given by

$$\vec{x} = \{T_{\text{A}},\ T_{\text{B}},\ \rho_{\text{A}},\ \rho_{\text{B}},\ y_1,\ \dot{y}_1,\ y_2,\ \dot{y}_2\} \tag{21}$$

$$\dot{\vec{x}} = \left\{\frac{\mathrm{d}T_{\text{A}}}{\mathrm{d}t},\ \frac{\mathrm{d}T_{\text{B}}}{\mathrm{d}t},\ \frac{\mathrm{d}\rho_{\text{A}}}{\mathrm{d}t},\ \frac{\mathrm{d}\rho_{\text{B}}}{\mathrm{d}t},\ \frac{\mathrm{d}y_1}{\mathrm{d}t},\ \frac{\mathrm{d}\dot{y}_1}{\mathrm{d}t},\ \frac{\mathrm{d}y_2}{\mathrm{d}t},\ \frac{\mathrm{d}\dot{y}_2}{\mathrm{d}t}\right\} \tag{22}$$

Equivalently, the derivatives with respect to the crank angle may be used in place of the derivatives with respect to time.

3.1. Numerical integrators

There are a multitude of numerical integrators that may be used to integrate a system of non-linear differential equations. Numerical integrators for systems of differential equations can be generally classified based on the following taxonomy:

- Explicit/implicit
- Single-step/multi-step
- Fixed-step-size/adaptive-step-size
- Order of truncation error

The selection of the best integrator for the simulation of a given machine is largely problem dependent and iterative. If no further knowledge is available, it is recommended to use the adaptive Runge-Kutta integrator. Three of the most-successful methods that have been implemented in PDSim are presented below.

3.1.1. Simple Euler Integrator

In the simple Euler integrator, the derivatives are evaluated at the current step $(t_{\rm old}, \vec{x}_{\rm old})$, and new values of the state variable $(\vec{x}_{\rm new})$ are predicted based on a linear extrapolation of the derivatives at this point. This can be expressed as

$$\vec{x}_{\rm new} = \vec{x}_{\rm old} + hf(t_{\rm old}, \vec{x}_{\rm old}), \tag{23}$$

which is a fixed step-size method, and exhibits error that is on the order of the step size to the first power. This method is quite simple to implement although it often struggles with severe numerical instabilities due to the stiffness of the system of differential equations.

3.1.2. Heun's Integrator

Heun's integrator, also known as the improved Euler rule, or the modified Euler rule, is a predictor-corrector method. The new state variable array $\vec{x}_{\rm new}$ is predicted with the same first step as in the simple Euler integrator, and the corrected step is obtained from an average of the derivatives at the beginning and predicted values:

$$\begin{aligned} \vec{x}^*_{\rm new} &= \vec{x}_{\rm old} + hf(t_{\rm old}, \vec{x}_{\rm old}) \\ \vec{x}_{\rm new} &= \vec{x}_{\rm old} + \frac{h}{2}\left[f(t_{\rm old}, \vec{x}_{\rm old}) + f(t_{\rm old}+h, \vec{x}^*_{\rm new})\right] \end{aligned}, \tag{24}$$

which yields an error that is on the order of the step size to the second power.

3.1.3. Adaptive Runge-Kutta Integrator

The simple integrators are not robust enough to handle some positive displacement machines. For instance, in scroll compressors it is common for the system of differential equations to be very stiff, requiring a very large number of steps in order to avoid numerical oscillations. Adaptive methods can more easily solve stiff system of differential equations, particularly when the the stiffness varies over a rotation. A complete description of the adaptive Runge-Kutta 4/5 method is provided as supplemental information in

The adaptive Runge-Kutta integrator handles stiff systems of equations with relative ease, though it is more complex to implement than Heun's Integrator or the Simple Euler Integrator. In addition, the adaptive Runge-Kutta method can tailor the step-size to the instantaneous requirements in order to maintain the required error per step with the minimum of computational effort.

4. Overall model

The preceding sections described the components that comprise most positive displacement compressors and expanders. A complete simulation model is constructed by taking component models out of the pool of components and connecting them together (numerically). The solvers involved in the simulation are then also connected numerically.

The model is constructed with one or more lumped masses that represent all the thermal inertia in the system, as shown in Figure

In the simulation, the exhaust pressure is specified, but the discharge temperature (or equivalently, the enthalpy) is unknown and must be determined iteratively. Therefore, the second independent variable in the simulation is the discharge enthalpy. In practice, the overall energy balance is enforced by solving the exhaust flow path backwards and back-calculating the enthalpy of the fluid leaving the set of chambers. The residual is the difference in the enthalpy between the back-calculated enthalpy and the outlet enthalpy of the set of chambers from the simulation. This discharge enthalpy from the chambers is calculated by carrying out the integrals in the equation

$$h_{\rm d,chambers} = \frac{\int_{\rm d} \dot{m}_i h_i}{\int_{\rm d} \dot{m}_i} \tag{25}$$

over the entire cycle (Bell, 2011).

Thus, the outer solver's role is to enforce energy balances on each of the lumped masses and determine the outlet temperature of the machine based on a global energy balance. This solver also includes preconditioning and post-processing steps. Figure

4.1. Solving

Figure

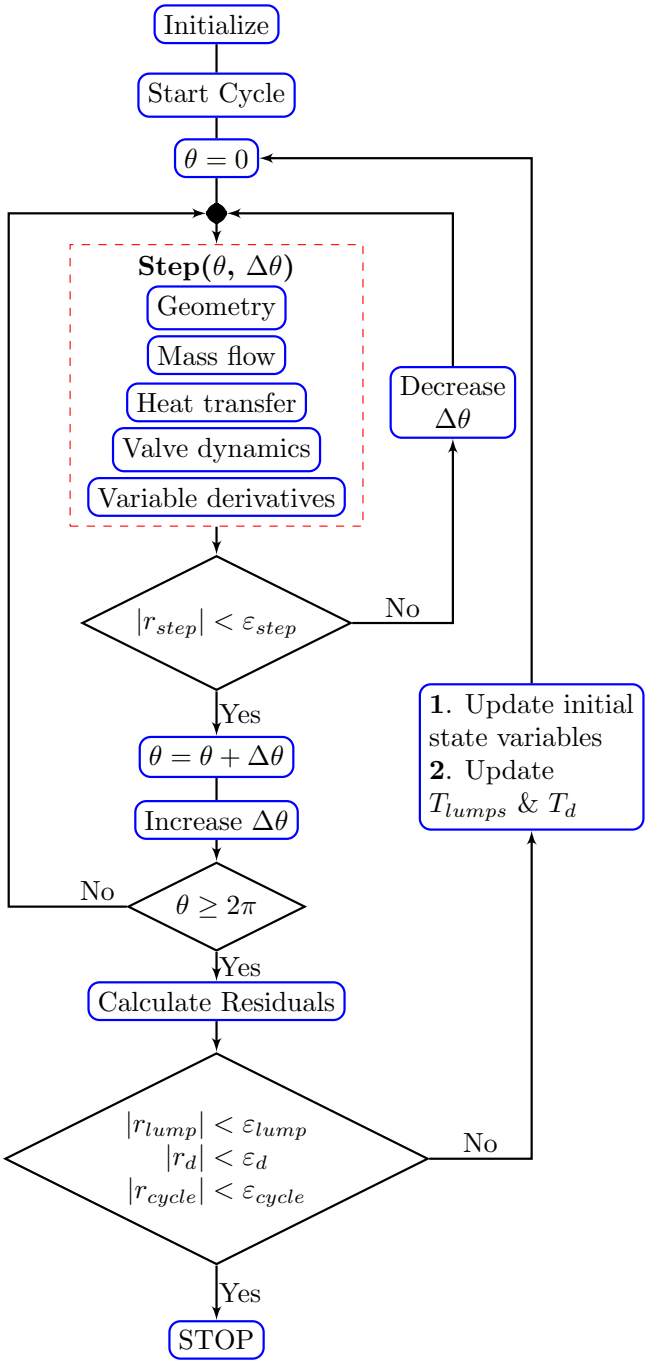

Figure 7: Flow chart of simulation in PDSim

With the initial guess for the lump mass temperatures and initial volume conditions set, the tubes are calculated in order to determine the tube pressures and enthalpies with which the control volumes will interact.

The overall solver is then executed. It enforces energy balances on each of the lumped masses by adjusting the lumped mass temperatures through the use of a non-linear system of equations solver.

At each step of the overall solver, the continuity solver is executed. Within the continuity solver, the cycle is run numerous times. Within the cycle, the integrator is used to calculate the values over one cycle. The integrator integrates the values obtained from one step. Once all the residuals are minimized, a steady-periodic dynamic solution is determined.

The hierarchical and nested behavior of the solvers result in a simulation algorithm that is fairly complex, though it is straightforward to simulate simple machines like a one-cylinder reciprocating compressor.

4.2. Continuity solver

When the machine has reached steady-state operation, the state variables for each control volume (as well as for any valves) will be equal at the beginning and the end of the cycle. In the simulation, this continuity must be enforced numerically, by active or passive means. Passive control uses the value of the state variables at the end of a cycle as values at the beginning of the next cycle. Active control includes applying a numerical technique as feedback for the next cycle to reduce the number of iterations. These include Brent's method (Brent, 1971) or the Newton-Raphson method as described in the following section. Here we have assumed that an array of state variables $\vec{x}_0$ is available at the beginning of the rotation.

The first category of methods are passive methods that are based on beginning the next cycle at the state given by the end of the prior cycle. In this method, the state variable array continuity is enforced by repetitively resetting the initial values for the state variables. If $\vec{x}_{\text{end}}$ is the end of one cycle and $\vec{x}_{\text{start}}$ is the state array at the start of the following cycle, $\vec{x}_{\text{start}}$ is set to be equal to $\vec{x}_{\text{end}}$ until $|\vec{x}_{\text{start}} - \vec{x}_{\text{end}}|$ is less than the desired tolerance.

In the second category are active methods that use numerical solvers of multi-dimensional non-linear systems of equations in order to enforce continuity between cycles. Selection of the active or passive method is problem specific. If there are a large number of control volumes, building the Jacobian matrix is extremely computationally expensive and it is preferable to use the passive method, even though it takes quite a few cycles to reach adequate convergence. For instance, in scroll compressors there can be as many as 10 or 15 control volumes (20-30 state variables in

total), and convergence is usually achieved in fewer than 30 cycles.
If, on the other hand, there is a large disparity in thermal inertia between control volumes, the active method is preferable as it short-cuts the convergence process of the chamber with the slow time constant. This disparity in thermal inertia is commonly experienced in the case of a residential refrigerator compressor where the shell volume is much greater than the volume of the working chamber. As a result, the time constant of the shell volume is large due to its relatively large mass, and the passive method experiences very slow convergence.

5. PDSim Framework

In the following sub-sections, the details of the implementation of PDSim are described.

5.1. Implementation

PDSim has been developed in the Python programming language with support for both 2.x and 3.x versions. The adoption of Python is justified by its open-source and cross-platform nature, the numerous packages available and the active community. PDSim takes advantage of both the high-level features of Python as well as the low-level code through Cython (Behnel et al., 2011) to achieve higher computational efficiency. PDSim is coded in an object-oriented fashion that ensures a plug-and-play structure that simplifies the construction of a model and facilitates the extension of the existing libraries. Additionally, PDSim integrates GUI (Graphical User Interface) development through the wxPython package. Furthermore, CoolProp and PDSim are linked at a very low level, allowing for minimal call overhead when evaluating thermophysical properties.
Each family of positive displacement machines represents a class in PDSim that can be used to build a specific compressor or expander model. General pseudocode of a simulation model in PDSim is shown in Figure

```
# Instantiate the model
comp = CompressorClass()
# Define the inputs}
# For example: comp.Vdead = 0.5e-5}
# Define boundary conditions}
Ref='Air'
inletState = State(Ref, T=298.15, P=101.325)
outletState = State(Ref, P=2*inletState.P, S=inletState.S)
mdot_guess = inletState.rho*comp.Vdisp*comp.omega/(2*pi)
# Add control volume(s)
comp.add_CV(ControlVolume(
    'CV', inletState, VdVFcn, becomes
))
# Add inlet tube
comp.add_tube(Tube(
    key1='inlet.1', key2='inlet.2', L, D,
    mdot=mdot_guess, State1=inletState,
    fixed=1, TubeFcn=comp.TubeCode
))
# Add outlet tube
comp.add_tube(Tube(
    key1='outlet.1', key2='outlet.2', L, D,
    mdot=mdot_guess, State2=outletState,
    fixed=2, TubeFcn=comp.TubeCode
))
# Add flow paths to connect flows
comp.add_flow(FlowPath('inlet.2','CV',MdotFcn))
comp.add_flow(FlowPath('CV','outlet.1',MdotFcn))
# Connect all the callbacks
comp.connect_callbacks(
    endcyle_callback=comp.endcycle_callback,
    heat_transfer_callback=comp.heat_transfer_callback,
    lump_energy_callback=comp.lump_energy_callback
)
# Run the solver
comp.solve(
    key_inlet='inlet.1',
    key_inlet='outlet.2',
    solver_method='RK45',
    OneCycle = False,
    UseNR = False
    )
```

Figure 8: Compressor pseudo-code in a Python-like style

The model for a particular machine is constructed as a class derived from the abstract base class `PDSimCore` (located at `PDSim/core/core.py`) in order to inherit a number of generic methods. For more detailed examples, please see the code provided in the supporting information and the examples provided in the companion paper Ziviani et al. (2019). The general methods used to construct all models are:

- `add_CV`: add the control volumes. Each `ControlVolume` instance is a class which contains methods for evaluating the volume and volume derivative with the crank angle. Each Control volume (there can be many of them) is added in this fashion, and is assigned a unique alphanumeric key.
- `add_flow`: add the flow paths (inlet and outlet flows, suction and discharge flows, leakage flows). These `FlowPath` classes contain the names of the entities (control volumes or tubes) that are connected by the flow model, and the flow function defines the flow model between the flow nodes.
- `add_tube`: add inlet and outlet tubes of the compressor/expander as well as possible injection lines; the `Tube` class contains the names of the flow nodes connected by the tube, and the flow model that handles the combination of heat transfer and pressure drop.
- `add_valves`: add valves, if any. The `Valve` class is integrated along with the control volumes and handles the dynamics of the valve lifting and closure.

– `connect_callbacks`: connect the callback functions. The callback functions are used to carry out calculations including the evaluation of the residual on the energy balance, any evaluations to be done at the end of one rotation, etc..
– `solve`: actually solve the model. The previous methods are used to configure the model, and `solve` runs the model. Solving repetitively runs the cycles and enforces energy balance on the lump, cycle-to-cycle convergence, and the overall energy balance on the machine.

The source code of PDSim consists of three main folders:

– `PDSim`: holds all the core elements to build a model and the different classes of PD machines. The PDSim folder includes the following subfolders:
  * `core`: includes the core elements of PDSim (e.g. governing equations, overall solution scheme, general methods);
  * `flow`: includes all the flow models and flow path methods;
  * `misc`: includes miscellaneous items that can be useful while developing models;
  * `plot`: includes the plotting classes for the debug plot features of PDSim;
  * `recip`: includes the reciprocating machine core class;
  * `rolling`: includes the rolling-piston machine core class;
  * `scroll`: includes the scroll machine core class;
– `GUI`: includes the files for the graphical user interface.
– `examples`: includes the examples of compressors and expander codes.

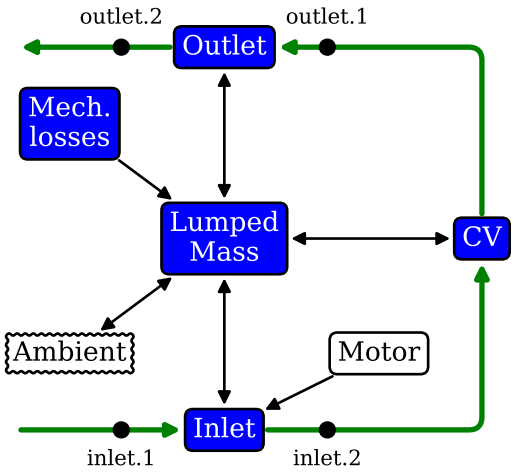

Table 4: List of geometric parameter of the reciprocating expander.

Parameter	Value
V_{disp}	100×10^{-6} m^3
V_{dead}	3×10^{-6} m^3
D_{port}	0.02 m
A_{shell}	0.405 m^2

6. Example of a reciprocating expander

As an example, the simulation framework described above is applied to a single-cylinder reciprocating expander designed for small-scale organic Rankine cycle (ORC) applications (Wronski, 2015). The analysis of this hypothetical expander is simplified for illustrative purposes in order to demonstrate some of the numerical and practical issues involved in the simulation of positive displacement machines and the source code is provided as supplementary material. The following simplifications are introduced in the model:

– No leakages or in-cylinder heat transfer.
– Constant mechanical losses.
– Heat transfer coefficient between expander shell and ambient, h_{amb}, is set equal to 0.01 kW m^{-2} K^{-1}.

The addition of models for the mechanical losses, leakages, and heat transfer is straightforward, but beyond the scope of this simplified example.
The geometric characteristics of the expander considered are listed in Table
Poppet valves are considered rather than reed valves because the pressure at the inlet is greater than that at the outlet port. Reed valves would not allow the expander to operate as desired. The geometry selected for the poppet valves is simplified and the valves are given sinusoidal flow area profiles with the crank angle as shown in Figure

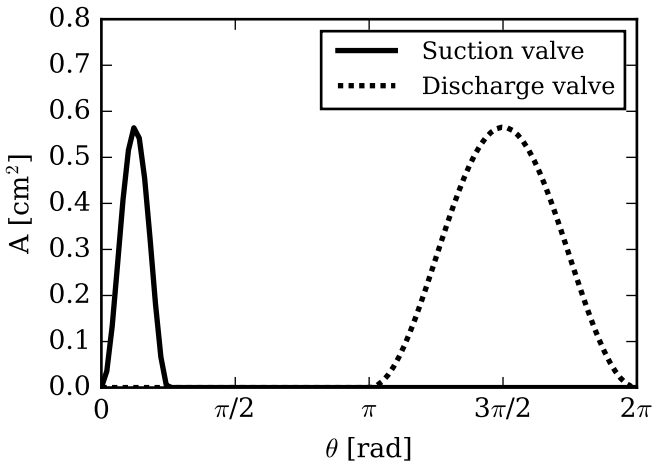

Figure 10: Valve flow area profiles during one crankshaft revolution.

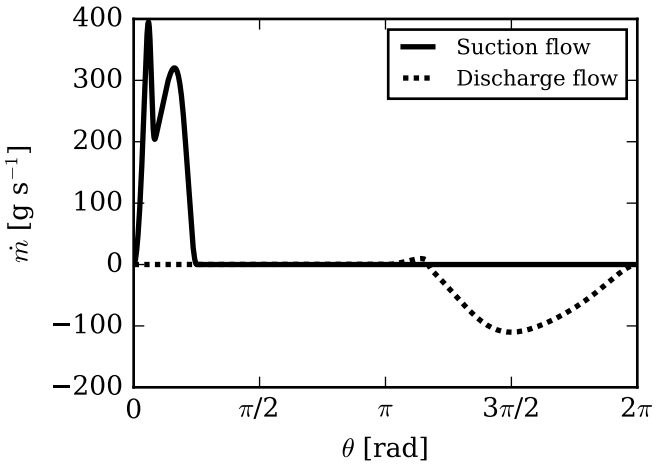

Figure 11: Mass flow rate through inlet and outlet ports. A negative flow value implies a flow rate *out* of the control volume

The average boundary work rate generated by the expander is calculated as

$$\overline{\dot{W}}_{pV} = \frac{\omega}{2\pi}\int_0^{2\pi} p(\theta)\frac{\mathrm{d}V}{\mathrm{d}\theta}\mathrm{d}\theta \tag{26}$$

The mechanical power output of the expander is obtained by subtracting the mechanical losses from the boundary work:

$$\dot{W}_{\mathrm{mech}} = \overline{\dot{W}}_{pV} - \dot{W}_{\mathrm{mech,loss}} \tag{27}$$

where the mechanical losses are assumed to be 20% of the boundary work rate. Note that the mechanical losses are subtracted from the boundary work only because this example represents an expander, for a compressor the mechanical losses would need to be added to the boundary work. The isentropic efficiency of the expander is calculated as the ratio of the mechanical shaft power to the isentropic power:

$$\eta_{\mathrm{s,mech}} = \frac{\dot{W}_{\mathrm{mech}}}{\dot{W}_{\mathrm{s}}} = \frac{\dot{W}_{\mathrm{mech}}}{\dot{m}\left[h_{\mathrm{in}}(T_{\mathrm{in}}, p_{\mathrm{in}}) - h_{\mathrm{out,s}}(p_{\mathrm{out}}, s_{\mathrm{in}})\right]} \tag{28}$$

where $\dot{m}$ is the mass flow rate displaced by the expander, $(p_{\mathrm{in}}, T_{\mathrm{in}})$ represent the supply pressure and temperature conditions, s_{in} is the specific entropy evaluated at the expander inlet conditions and p_{out} is the discharge pressure.
The residual of discharge enthalpy over one cycle is obtained from

$$\overline{h}_{\mathrm{d,Cycle}} - h_{\mathrm{d}} = 0 \tag{29}$$

and the overall energy balance is given by,

$$\dot{W}_{\mathrm{mech,loss}} + \sum_i \dot{Q}_i(T_{\mathrm{lump}}) = 0 \tag{30}$$

where T_{lump} is the mean temperature of the lumped mass of the expander shell and $\dot{Q}_i$ represents all the heat transfer interaction terms between the different parts of the expander and the shell. In this case, only the heat transfer between shell and the ambient is accounted for, i.e.,

$$\sum_{i=1} \dot{Q}_i = \dot{Q}_{\mathrm{amb}} = h_{\mathrm{amb}} A_{\mathrm{shell}}(T_{\mathrm{amb}} - T_{\mathrm{lump}}) \tag{31}$$

where T_{amb} is the ambient temperature.
The simulation is set up by imposing the inlet temperature and pressure values as well as the discharge pressure or the pressure ratio across the expander. The working fluid considered is refrigerant R-245fa and its thermophysical properties are retrieved from CoolProp. The convergence history of the discharge state and the overall energy balance are illustrated in Figure

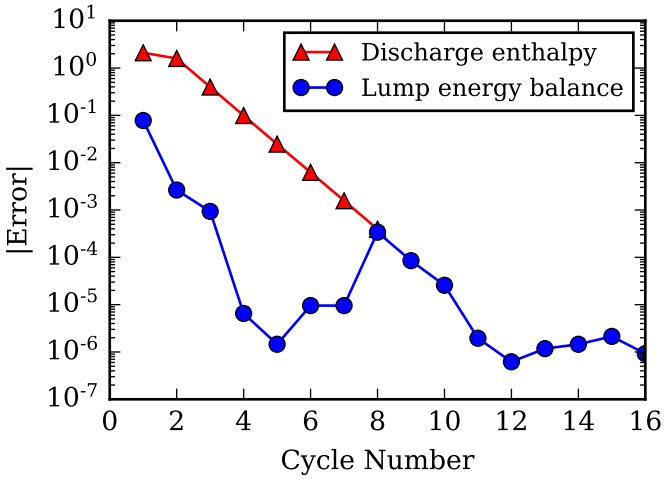

Figure 12: Convergence history of the residuals on discharge state and overall energy balance of the expander shell.

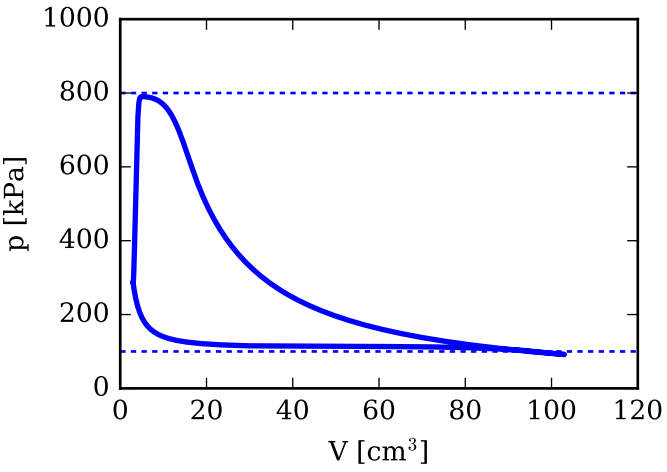

Figure 13: Expander pressure-volume diagram: $T_{\mathrm{su}} = 100$ °C, $p_{\mathrm{su}} = 800$ kPa, $r_{\mathrm{p}} = 8$ at 3600 rpm.

7. Conclusions

A general framework for the analysis of positive displacement compressors and expanders has been presented and implemented within a software package entitled PDSim (Positive Displacement SIMulation). The code is implemented in the programming language Python, with performance-critical components implemented in cython (Behnel et al., 2011). In this way, the high-level nature of Python can be maintained while achieving computational speeds equivalent to low-level programming languages like C++. The code is highly object-oriented, and Python is a modern programming language that allows for easy modification and extension. A reciprocating expander has been considered as a simple example to show the basic features of the software. Additional compressor models are available with the PDSim library and are discussed in the companion paper (Ziviani et al., 2019). PDSim represents the first open-source generalized software able to model any quasi-steady positive displacement machine.

Supporting Information

The Supporting Information of this paper includes:

- The source code of PDSim as of publication is archived on figshare at `https://doi.org/10.6084/m9.figshare.7985651`. The git repository with the most current code for PDSim is at `https://github.com/ibell/pdsim`
- The simple piston expander described in this paper.

References

Adair, R., Qvale, E., Pearson, J., 1972. Instantaneous heat transfer to the cylinder wall in reciprocating compressors, in: International Compressor Engineering Conference, pp. 521–526.

Afjei, T., Suter, P., Favrat, D., 1992. Experimental analysis of an inverter-driven scroll compressor with liquid injection, in: 1992 Compressor Engineering Conference at Purdue University.

Beard, J.E., 1985. Kinematic analysis of gerotor type pumps, engines, and compressors. Ph.D. thesis.

Behnel, S., Bradshaw, R., Citro, C., Dalcin, L., Seljebotn, D., Smith, K., 2011. Cython: The best of both worlds. Computing in Science Engineering 13, 31 –39. doi:10.1109/MCSE.2010.118.

Bell, I., 2011. Theoretical and Experimental Analysis of Liquid Flooded Compression in Scroll Compressors. Ph.D. thesis. Purdue University. URL: http://docs.lib.purdue.edu/herrick/2/.

Bell, I.H., Groll, E.A., Braun, J.E., Horton, W.T., 2013. A computationally efficient hybrid leakage model for positive displacement compressors and expanders. Int. J. Refrig. doi:10.1016/j.ijrefrig.2013.01.005.

Bell, I.H., Lemort, V., Groll, E.A., Braun, J.E., King, G.B., Horton, W.T., 2012. Liquid flooded compression and expansion in scroll machines – part II: Experimental testing and model validation. International Journal of Refrigeration 35, 1890–1900. doi:10.1016/j.ijrefrig.2012.07.008.

Bell, I.H., Wronski, J., Quoilin, S., Lemort, V., 2014. Pure and Pseudo-pure Fluid Thermophysical Property Evaluation and the Open-Source Thermophysical Property Library CoolProp. Industrial & Engineering Chemistry Research 53, 2498–2508. doi:10.1021/ie4033999.

Bianchi, G., Cipollone, R., 2015. Friction power modeling and measurements in sliding vane rotary compressors. Applied Thermal 84, 276–285.

Bianchi, G., JKennedy, S., Zaher, O., Tassou, S.A., Miller, J., Jouhara, H., 2018. Numerical modeling of a two-phase twin-screw expander for Trilateral Flash Cycle applications 88, 248–259.

Blevins, R.D., 1979. Formulas for Natural Frequency and Mode Shape. van Nostrand Reinhold Company.

Bradshaw, C., 2012. A Miniature-Scale Linear Compressor for Electronics Cooling. Ph.D. thesis. Purdue University.

Bradshaw, C.R., Groll, E.A., 2013. A comprehensive model of a novel rotating spool compressor. International Journal of Refrigeration 36, 1974–1981.

Bradshaw, C.R., Groll, E.A., Garimella, S.V., 2011. A comprehensive model of a miniature-scale linear compressor for electronics cooling. International Journal of Refrigeration 34, 63 – 73. doi:10.1016/j.ijrefrig.2010.09.016.

Bradshaw, C.R., Kemp, G., Orosz, J., Groll, E.A., 2016. Development of a loss pareto for a rotating spool compressor using high-speed pressure measurements and friction analysis. Applied Thermal Engineering 99, 392–401.

Brent, R., 1971. An algorithm with guaranteed convergence for finding a zero of a function. The Computer Journal 14, 422–425.

Cash, J., Karp, A.H., 1990. A Variable Order Runge-Kutta Method for Initial Value Problems with Rapidly Varying Right-Hand Sides. ACM Transactions on Mathematical Software 16, 201–222.

Chapman, S.J., 2005. Electric Machinery Fundamentals. McGraw Hill.

Chen, Y., Halm, N., Groll, E., Braun, J., 2002a. Mathematical Modeling of Scroll Compressor. Part I- Compression Process Modeling. Int. J. Refrig. 25, 731–750.

Chen, Y., Halm, N., Groll, E., Braun, J., 2002b. Mathematical Modeling of Scroll Compressor. Part II- Overall scroll compressor modeling. Int. J. Refrig. 25, 751–764.

Churchill, S., 1977. Friction factor equation spans all fluid flow regimes. Chemical Engineering 84, 91–92.

Fransesconi, M., Antonelli, M., 2017. A numerical model for the prediction of the fluid dynamic and mechanical losses of a Wankel-type expansion device 205, 225–235.

Galindo, J., Dolz, V., Royo-Pascual, L., Haller, R., Melis, J., 2016. Modeling and Experimental Validation of a Volumetric Expander Suitable for Waste Heat Recovery from and Automotive Internal Combustion EEngine Using an Organic Rankine Cycle with Ethanol 9, 1–18.

Gnielinski, V., 1975. Neue gleichungen für den wärme-und den stoffübergang in turbulent durchströmten rohren und kanälen. Forschung im Ingenieurwesen 41, 8–16.

Hamrock, B.J., Schmid, S.R., Jacobson, B.O., 2004. Fundamentals of Fluid Film Lubrication. CRC Press.

Hu, J., Yang, L., Shao, L.L., Zhang, C.L., 2014. Generic network model of reciprocating compressor. Int. J. Refrig. 45, 107–119.

Ishii, N., Bird, K., Sano, K., Oono, M., Iwamura, S., Otokura, T., 1996. Refrigerant Leakage Flow Evaluation for scroll compressors, in: 1996 Compressor Conference at Purdue University.

Jovane, M., 2007. Modeling and analysis of a novel rotary compressor. Ph.D. thesis. Purdue University.

Kakaç, S., Shah, R.K., Aung, W., 1987. Handbook of single-phase convective heat transfer. Wiley New York et al.

Kim, H., Roh, C.g., Kim, J.k., Shin, J.m., Hwang, Y., Lee,

J.k., 2009. An experimental and numerical study on dynamic characteristic of linear compressor in refrigeration system 32, 1536–1543.

Kim, J.H., 2005. Analysis of a Bowtie Compressor with Novel Capacity Modulation. Ph.D. thesis. Purdue University.

Krishna, A., 2015. Analysis of a rotaring spool expander for organic Rankine cycle applications. Ph.D. thesis.

Lemmon, E., 2003. Pseudo-Pure Fluid Equations of State for the Refrigerant Blends R-410A, R-404A, R-507A, and R-407C. Int. J. Thermophys. 24, 991–1006.

Lemmon, E.W., Bell, I.H., Huber, M.L., McLinden, M.O., 2016. NIST Standard Reference Database 23: Reference Fluid Thermodynamic and Transport Properties-REFPROP, Version 9.1.1, National Institute of Standards and Technology.

Lemort, V., 2008. Contribution to the Characterization of Scroll Machines in Compressor and Expander Modes. Ph.D. thesis. University of Liège.

Lemort, V., Bell, I., Groll, E., Braun, J.E., 2008. Analysis of liquid-flooded expansion using a scroll expander, in: 19th Compressor Engineering Conference at Purdue University.

Link, R., Deschamps, C.J., 2011. Numerical modeling of startup and shutdown transients in reciprocating compressors. International Journal of Refrigeration 34, 1398–1414.

Liu, R., Zhou, Z., 1984. Heat transfer between gas and cylinder wall of refrigerating reciprocating compressor, in: International Compressor Engineering Conference, pp. 110–115.

Liu, Y., Hung, C., Chang, Y., 2010. Design optimization of scroll compressor applied for frictional losses evaluation. Int. J. Refrig. 33, 615 – 624. doi:10.1016/j.ijrefrig.2009.12.015.

Mathison, M.M., Braun, J.E., Groll, E.A., 2008. Modeling of a two-stage rotary compressor. HVAC&R Research 14, 719–748.

Mathison, M.M., Braun, J.E., Groll, E.A., 2013. Modeling of a novel spool compressor with multiple vapor injection ports. Int. J. Refrig. 3t6, 1982–1997.

Nikolov, A., Brummer, A., 2017. Investigating a Small Oil-Flooded twin-Screw Expander for waste-Heat Utilisation in Organic Rankine Cycle Systems. Energies 10, 1–27.

Okada, K., Kuyama, K., 1982. Motion of Rolling Piston in Rotary Compressor, in: International Compressor Engineering Conference at Purdue University.

Ooi, K., Wong, T., 1997. A computer simulation of a rotary compressor for household refrigerators. Applied Thermal Engineering 17, 65–78.

Oudkerk, J.F., 2016. Contribution to the Characterization of Piston Expanders for their Use in Small-Scale Power Production Systems. Ph.D. thesis.

Pan, X., Wang, M., Xing, Z., Shulin, p., 2018. Structural study on a swing compressor with no valves for air conditioning systems 88, 300–306.

Papes, I., Degroote, J., Vierendels, J., 2016. Development of a thermodynamic loworder model for a twin-screw expander with emphasis on pulsations in the inlet pipe. Applied Thermal Engineering 103, 909–919.

Pérez, F., Granger, B.E., 2007. IPython: a system for interactive scientific computing. Computing in Science and Engineering 9, 21–29. doi:10.1109/MCSE.2007.53.

Raimondi, A., Boyd, J., 1958a. A Solution for the Finite Journal Bearing and its Application to Analysis and Design: I. A S L E Transactions 1, 159–174. doi:10.1080/05698195808972328.

Raimondi, A., Boyd, J., 1958b. A Solution for the Finite Journal Bearing and its Application to Analysis and Design: II. A S L E Transactions 1, 175–193. doi:10.1080/05698195808972329.

Raimondi, A., Boyd, J., 1958c. A Solution for the Finite Journal Bearing and its Application to Analysis and Design: III. A S L E Transactions 1, 194–209. doi:10.1080/05698195808972330.

Sathe, A.A., 2008. Miniature-scale Diaphragm Compressor for Electronics Cooling. Ph.D. thesis.

Schiffmann, J., 2014. Small-scale and oil-free turbocompressor for refrigeration applications, in: International Compressor Engineering Conference.

Shung, J.B., Pennock, G.R., 1994. Geometry for Trochoidal-Type Machines with Conjugate EEnvelope 29, 25–42.

Singh, P.J., 1984. A digital reciprocating compressor simulation program including suction and discharge piping, in: International Compressor Engineering Conference at Purdue 1984.

Soedel, W., 1984. Design and Mechanics of Compressor Valves. Ray W. Herrick Laboratories, School of Mechanical Engineering, Purdue University.

Soedel, W., 2007. Sound and Vibrations of Positive Displacement Compressors. CRC Press Taylor & Francis Group.

Stosic, N., Smith, I.K., Kovacevic, A., Mujic, E., 2011. Review of Mathematical Models in Performance Calculation of Screw Compressors. International Journal of Fluid Machinery and System 4, 271–288.

Suefuji, K., Nakayama, S., 1980. Practical method for analysis and estimation of reciprocating hermetic compressor performance, in: International Compressor Engineering Conference at Purdue University.

Suefuji, K., Shiibayashi, M., Tojo, K., 1992. Performance analysis of hermetic scroll compressors, in: 1992 International Compressor Engineering Conference at Purdue University.

Tan, K., Ooi, K., 2011. Heat transfer in compression chamber of a revolving vane (rv) compressor. Applied Thermal Engineering 31, 1519–1526.

Tian, C., Dou, C., Yang, X., Li, X., 2004. A mathematical model of variable displacement wobble plate compressor for automotive air conditioning system 24, 2467–2486.

Tojo, K., Ikegawa, M., Maeda, N., Machida, S., Shiibayashi, M., Uchikawa, N., 1986. Computer modeling of scroll compressor with self adjusting back-pressure mechanism, in: 1986 International Compressor Engineering Conference at Purdue University.

Wang, Z., Shen, Y., Wang, Z., Wang, J., Jiang, W., Li, Q., 2018. Theoretical research and optimization analysis for the injection process of the single screw refrigeration compressor. Int. J. Refrig. 88, 91–101.

Wronski, J., 2015. Design and Modelling of Small Scale Low Temperature Power Cycles. Ph.D. thesis. Technical University of Denmark.

Wu, Y.R., Tran, V.T., 2016. Dynamic response prediction of a twin-screw compressor with gas-induced cyclic loads based on multi-body dynamics. International Journal of Refrigeration 65, 111–128.

Yanagisawa, T., Shimizu, T., 1985. Friction losses in rolling piston type rotary compressors. III. Int. J. Refrig. 8, 159 – 165. doi:10.1016/0140-7007(85)90156-2.

Yang, B., Bradshaw, C.R., Groll, E.A., 2013. Modeling of a semi-hermetic CO_2 reciprocating compressor including lubrication submodels for piston rings and bearings. Int. J. Refrig. 36, 1925–1936.

Yang, B., Kurtulus, O., Groll, E.A., 2015. Modeling of an Oil-Free Carbon Dioxide Compressor Using Sanderson-Rocker Arm Motion (S-RAM) Mechanism. IOP Conf. Ser.: Mater. Sci. Eng. 90.

Yang, X., Dong, C., Qu, Z., 2017. Design and dynamic analysis of a novel double-swing vane compressor for electric vehicle air conditioning systems. Int. J. Refrig. 76, 52–62.

Yap, K.S., ooi, K.T., Chakraborty, A., 2018. Analysis of the novel cross vane expander-compressor: Mathematical modelling and experimental study. Energy 145, 626–637.

Zaytsev, D., 2003. Development of Wet Compressor for Application in Compression-Resorption Heat Pumps. Ph.D. thesis.

Zhang, Y., Wang, W., 2011. Effect of leakage and friction on the miniaturization of a Wankel compressor. Front. Energy 5, 83–92.

Zhao, L., Li, M., Ma, Y., liu, Z., Zhang, Z., 2014. Simulation analysis of a two-rolling piston expander replacing a throttling valve in a refrigeration and heat pump system. Applied Thermal Engineering 66, 383–394.

Ziviani, D., 2017. Theoretical and Experimental Characterization of Single-Screw Expanders for ORC Applications. Ph.D. thesis.

Ziviani, D., Bell, I.H., Zhang, X., Lemort, V., De Paepe, M., Braun, J.E., Groll, E.A., 2019. Demonstrating the capabilities of an open-source simulation framework for positive displacement compressors and expanders. Int. J. Refrig. Submitted.

Ziviani, D., Groll, E., 2017. Modeling and analysis of an open-drive Z-compressor. IOP Conf. Ser.: Mater. Sci. Eng. 232.

Appendix A. Formulation of the adaptive Runge-Kutta 4/5 integration method

Adaptive methods estimate the local truncation error of a single Runge-Kutta (RK) step. The Butcher tableau includes two methods, one with order p and one with order $p-1$. For a given step size h, the adaptive Runge-Kutta method is employed with the coefficients from Cash and Carp (1990). This yields the following algorithm:

$$\vec{f_1} = f(t_{\text{old}}, \vec{x}_{\text{old}}) \tag{A.1}$$

$$\vec{x}_1 = \vec{x}_{\text{old}} + h\left(\frac{1}{5}\vec{f_1}\right) \tag{A.2}$$

$$\vec{f_2} = f\left(t_{\text{old}} + \frac{1}{5}h, \vec{x}_1\right) \tag{A.3}$$

$$\vec{x}_2 = \vec{x}_{\text{old}} + h\left(\frac{3}{40}\vec{f_1} + \frac{9}{40}\vec{f_2}\right) \tag{A.4}$$

$$\vec{f_3} = f\left(t_{\text{old}} + \frac{3}{10}h, \vec{x}_2\right) \tag{A.5}$$

$$\vec{x}_3 = \vec{x}_{\text{old}} + h\left(\frac{3}{10}\vec{f_1} - \frac{9}{10}\vec{f_2} + \frac{6}{5}\vec{f_3}\right) \tag{A.6}$$

$$\vec{f_4} = f\left(t_{\text{old}} + \frac{3}{5}h, \vec{x}_3\right) \tag{A.7}$$

$$\vec{x}_4 = \vec{x}_{\text{old}} + h\left(-\frac{11}{54}\vec{f_1} + \frac{5}{2}\vec{f_2} - \frac{70}{27}\vec{f_3} + \frac{35}{27}\vec{f_4}\right) \tag{A.8}$$

$$\vec{f_5} = f(t_{\text{old}} + h, \vec{x}_4) \tag{A.9}$$

$$\vec{x}_5 = \vec{x}_{\text{old}} + h\left(\frac{1631}{55296}\vec{f_1} + \frac{175}{512}\vec{f_2} + \frac{575}{13824}\vec{f_3} + \frac{44275}{110592}\vec{f_4} + \frac{253}{4096}\vec{f_5}\right) \tag{A.10}$$

$$\vec{f_6} = f\left(t_{\text{old}} + \frac{7}{8}h, \vec{x}_5\right) \tag{A.11}$$

The new values for the state variables $\vec{x}_{\text{new}}$ are given by

$$\vec{x}_{\text{new}} = \vec{x}_{\text{old}} + h\left(\frac{37}{378}\vec{f_1} + \frac{250}{621}\vec{f_3} + \frac{125}{594}\vec{f_4} + \frac{512}{1771}\vec{f_6}\right) \tag{A.12}$$

and an estimate of the error is given by

$$\frac{\vec{\epsilon}}{h} = -\frac{277}{64512}\vec{f_1} + \frac{6925}{370944}\vec{f_3} - \frac{6925}{202752}\vec{f_4} - \frac{277}{14336}\vec{f_5} + \frac{277}{7084}\vec{f_6} \tag{A.13}$$

If the maximum absolute error given by $\epsilon_{\max} = \max(|\vec{\epsilon}|)$ is less than the allowed error per step of $\epsilon_{\text{allowed}}$, the step is accepted, and the step size used was unnecessarily small, so the step size for the next step is increased using

$$h_{\text{next}} = 0.9h\left(\frac{\epsilon_{\text{allowed}}}{\epsilon_{\max}}\right)^{0.2} \tag{A.14}$$

If the error is too large ($\epsilon_{\max} > \epsilon_{\text{allowed}}$), the step must be tried again, but this time with a smaller step. The new step size is obtained from

$$h_{\text{next}} = 0.9h\left(\frac{\epsilon_{\text{allowed}}}{\epsilon_{\max}}\right)^{0.3} \tag{A.15}$$

The parameter 0.9 is a safety factor that forces the method to be conservative in its step resizing.
An example of using RK 4/5 integration method with a stiff equation is provided as a Jupyter (formerly known as an IPython (Pérez and Granger, 2007)) notebook.